# Coulomb Effects on Particle Spectra in Relativistic Nuclear Collisions

H.W. Barz[1], J.P. Bondorf[2], J.J. Gaardhøje[2], and H. Heiselberg[3]

[1] Forschungszentrum Rossendorf, Pf 510119, 01314 Dresden, Germany

[2]Niels Bohr Institute, Blegdamsvej 17, 2100 Copenhagen, Denmark

[3]NORDITA, Blegdamsvej 17, 2100 Copenhagen, Denmark

February 9, 2008

**Abstract:**

Coulomb effects on $\pi^{\pm}$ and $K^{\pm}$ spectra in relativistic nuclear collisions are investigated. At collision energies around 1 GeV the ratio of $\pi^-$ to $\pi^+$ is enhanced several times at low transverse momenta but less at ultrarelativistic energies. We describe the ratios at SIS, AGS and SPS energies with simple analytic models as well as more elaborate numerical models incorporating the expansion dynamics. The Coulomb effect depends on the properties of the source after the violent collision phase and provides information on source sizes, freeze-out times, and expansion velocities. Comparison with results from HBT analyses are made. Predictions for $\pi^{\pm}$ and $K^{\pm}$ at RHIC and LHC energies are given.

PACS numbers: 25.75.+r, 25.70.Pq

## I. INTRODUCTION

An asymmetry in the number of opposite charge pions has been observed at intermediate energies [1] and has recently also been identified in heavy ion collisions at energies around 1 $A$·GeV [2,3], 11.4 $A$·GeV [4], and 158 $A$·GeV [5]. The effect is strongest at lower beam energies. The ratio of negative to positive pions at low pion momenta is $\sim 3$ at SIS energies, but only $\sim 1.6$ at AGS and SPS energies for the central collisions of heavy nuclei as $Au$ or $Pb$. A possible cause for this effect is the Coulomb interaction between the produced pions and the positive charge from the reaction partners.

Earlier work [6–9] has described the $\pi^-/\pi^+$ enhancement/reduction by Coulomb attraction/repulsion from a static source. In this paper we underline the importance of the source dynamics and of the longitudinal and transverse expansion of the fireball. We emphasize the different reaction kinematics and dynamics that evolve from 1 $A$·GeV to 160 $A$·GeV. At the lower collision energies nuclear matter is fully stopped and expands relatively slowly in all

directions whereas at higher energies much of the initial motion survives and the system expands faster preferentially in longitudinal direction.

Since the Coulomb forces influence the matter essentially after freeze-out, the asymmetry in the number of differently charged particles can be directly related to the freeze-out parameters of the matter. Therefore, a detailed description of the violent initial part of the collision is unnecessary, and it is sufficient to consider the state of the nuclear matter at the time $\tau_f$ of freeze-out. Similar to particle interferometry measurements the observation of Coulomb effects can help to determine the dynamics of heavy ion collisions.

We will develop approximate models by assuming simple geometrical shapes of the charge distribution at freeze-out. In these models we can estimate analytically the ratio of $\pi^-$ to $\pi^+$ as a function of the transverse momentum. In an earlier publication [10] we have presented a model of an expanding pion gas created in heavy ion collisions at ultrarelativistic energies. This model is well applicable in a wide range of collision energies. We will use it for calculating particle ratios as a check of the simpler models.

The manuscript is organized as follows. In section II we study slowly expanding and spherically symmetric sources from which pions escape rapidly. Such a scenario may be applicable to heavy ion collisions around 1 $A$·GeV and we compare to SIS data. In section III, we study rapidly expanding systems from nuclear collisions at ultrarelativistic energies, which may apply to collisions at the AGS and SPS. We compare to recent AGS and SPS data. In section IV we investigate the situation for particles at very low momentum. In section V we briefly overview the main ingredients of the dynamical model developed in ref. [10] and compare. In section VI we compare freeze-out radii to those obtained from HBT analyses. In section VII we discuss the influence of particles created at late stages from resonance decays, and in section VIII we consider $K^-/K^+$ ratios. Finally, predictions for charged pion and kaon ratios at RHIC and LHC energies are given.

## II. SLOWLY EXPANDING CHARGE

In nuclear collisions charged particles feel a Coulomb force due to the net positive charge originating form the protons in the colliding nuclei. In particular the light produced particles as $\pi^\pm, K^\pm, ...$ moving slowly with respect to the net positive charge are significantly affected by the Coulomb field. We will concentrate on pions, which are affected strongest by the Coulomb field since they are the lightest particles, but all results apply to any particle of mass $m$ as, e.g., kaons or protons.

The net charge of the source resides mainly in protons also after the collisions. Expansion of the "cloud of charge" can thus be considered slow when typical proton velocities $v_p$ are much smaller than pion velocities $v_\pi$. At SIS energies the energies of protons from central collisions and at midrapidity follow approximately a Boltzmann distribution with temperature $T_p \simeq 100$ MeV [11]. Only slow pions with $v_\pi < v_p$ are affected while for pions with kinetic energies*

$$\frac{1}{2} m_\pi \langle v_\pi^2 \rangle \; > \; \frac{1}{2} m_\pi \langle v_p^2 \rangle \simeq \frac{3}{2} T_p \frac{m_\pi}{m_p} \tag{1}$$

*We will in the following use the convention $\hbar = c = k_B = 1$.

the expansion can be ignored. At SIS energies this limit is thus $\sim 20$ MeV and Eq. (1) applies to all SIS data shown in Fig. 1. Thus the charge expansion can be ignored for the SIS data.

Let us therefore consider a particle $(\pi^{\pm}, K^{\pm}, ...)$ with mass $m$ and energy $E_0 = \sqrt{m^2 + p_0^2}$ which is formed in a spherically symmetric source with net charge $Z$ evenly distributed over the volume of radius $R$. We will for the moment assume that the charge is static and will later extend the analysis to an expanding charge. The Coulomb potential varies from $Ze^2/R$ at the surface to 3/2 times that value at the center with the average

$$V_c = \frac{6}{5}\frac{Ze^2}{R}\,. \tag{2}$$

The energy and momenta of $\pi^0$'s are unaffected by the Coulomb field and define the reference values, $E_0$ and $p_0$, whereas the $\pi^{\pm}$ are accelerated/decelerated in the field. As the volume expands slowly with respect to the fast pions, the final $\pi^{\pm}$ energy is

$$E = E_0 \pm V_c\,. \tag{3}$$

The effect on the particle distribution functions can be derived from particle conservation, i.e., the number of particles before Coulomb effects are not changed after, $dN_0$=$dN$. The $\pi^{\pm}$ pion distributions at freeze-out $d^3N_0/d^3p_0$ now have to be transformed by changing their energy and momentum following (3). The final distribution is

$$\frac{dN}{d^3p} = \frac{dN_0}{d^3p_0}\frac{d^3p_0}{d^3p} = \frac{dN_0}{d^3p_0}\frac{p_0}{p}\frac{E_0}{E}\,. \tag{4}$$

The original $dN^0/d^3p_0$ can be taken from $\pi^0$ data around 1 GeV. These pion spectra are to a good approximation given by $dN^0/d^3p_0 \sim \exp(-E_0/T)$ with slope parameter $T$. With final $\pi^{\pm}$ energy and momentum given by (3) and using (4) for both $\pi^-$ and $\pi^+$, one obtains the ratio (see also [8,12])

$$\frac{\pi^-}{\pi^+} \equiv \frac{dN^-/d^3p}{dN^+/d^3p} \quad = \langle\frac{\pi^-}{\pi^+}\rangle \exp\left(-\frac{2V_c}{T}\right)\,\frac{E+V_c}{E-V_c}\,\sqrt{\frac{(E+V_c)^2-m^2}{(E-V_c)^2-m^2}}\,. \tag{5}$$

The square root denotes the ratio of the initial $\pi^-$ and $\pi^+$ momenta when they are detected with final energy $E$. It leads to diverging rate as the kinetic energy $(E-m)$ approaches $V_c$, $\pi^-/\pi^+ \propto (E-m-V_c)^{-1/2}$. The average $\langle\pi^-/\pi^+\rangle$ is the ratio of the total number of negative and positive pions produced. At collisions energies of 1 GeV most pions are produced through the $\Delta$ resonance, the ratio is [2,7]

$$\langle\frac{\pi^-}{\pi^+}\rangle = \frac{5N^2+NZ}{5Z^2+NZ} \simeq 1.94\,, \tag{6}$$

where $N$ and $Z$ are the neutron and proton numbers of the $Au+Au$ nuclei before collision.

The simple formula (5) gives a good description of the $\pi^+/\pi^-$ ratio for the 1 GeV $Au+Au$ collisions at SIS and allows us to determine both $T \simeq 75$ MeV and $V_c \simeq 27 \pm 2$ MeV, see Fig. 1. These two parameters can also be estimated independently. The measured single particle slope $T \simeq 75$ MeV [11] agrees nicely with our estimate. According to Eq. (2) the value of $V_c \simeq 27$MeV and $Z = 2 \times 79 \times 0.75$ (14 % centrality) corresponds to an average source size of $R \simeq 8.0$ fm, which is larger than the geometrical radius of the initial participant zone of the two colliding $Au$ nuclei.

The corresponding baryon density at pion freeze-out is $\sim 2A/(4\pi R^3/3) \simeq 0.85\rho_0$, i.e., somewhat smaller than normal nuclear matter density $\rho_0$. We will see that this result agrees with the investigations in the dynamical model described in section V. In the analysis of this data within the transport model [13] a similar value of the Coulomb energy was obtained, although at smaller density of $\sim 0.6\rho_0$.

## III. RAPIDLY LONGITUDINALLY EXPANDING SYSTEMS

At the higher AGS, SPS, RHIC and LHC energies the systems expands rapidly in particular in the longitudinal direction along the beam axis. For systems expanding more rapidly than the pion velocity the net charge is reduced with increasing time resulting in decreased Coulomb effects. At ultrarelativistic speeds one also needs to take retardation effects of the Coulomb fields into account.

Our starting point is the retarded time component of the electromagnetic potential from a charge $Q$ moving with velocity $v$ along the beam axis [14]

$$\phi(r_\perp, t) = A^0 = \frac{Q}{\sqrt{v^2 t^2 + (1-v^2) r_\perp^2}}, \tag{7}$$

where $r_\perp$ is the distance from the beam axis and the time is chosen such that $t = 0$ when the charge is closest to the point $r_\perp$ (see Fig. 2). The vector part of the potential points along $\mathbf{v}$ and is therefore longitudinal and does not contribute to the transverse electric field that affects transverse momenta. The longitudinal component even vanishes for an approximately constant rapidity distribution since the contributions of negative and positive velocities cancel each other.

In ultrarelativistic heavy ion collisions the charged particles have large longitudinal but small transverse momenta. The distribution of longitudinal velocities $v$ can be obtained from the measured rapidity distributions since $v = \tanh(y)$

$$\frac{dN^{ch}}{dv} = \frac{1}{1-v^2} \frac{dN^{ch}}{dy} \,. \tag{8}$$

In central $Pb + Pb$ collisions at SPS energies the net proton rapidity distribution is rather constant at midrapidities, $dN^{(p)}/dy = 37 \pm 2$ [15,16].

Assuming an approximately flat charge rapidity distribution, the electric field becomes

$$\begin{aligned} \mathbf{E}(r_\perp, t) = -\nabla\phi(r_\perp, t) &= e \int \frac{dN^{ch}}{dy} \frac{\mathbf{r}_\perp dv}{(r_\perp^2 + v^2(t^2 - r_\perp^2))^{3/2}} \\ &= e \frac{dN^{ch}}{dy} \frac{2}{t} \frac{\mathbf{r}_\perp}{r_\perp^2} \,. \end{aligned} \tag{9}$$

In relativistic heavy ion collisions the upper and lower velocities range from $\pm c$ .[†] In the Bjorken scaling picture [17] $t$ counts time from the moment $t = 0$ of the total overlap of the collision partners.

As can be seen from (7) the electric potential is dominated by the slow charges ($v \sim 0$) simply because they provide a Coulomb field for a longer time. Thus pions with rapidity $y$ mainly feel the Coulomb field from charged particles at similar rapidities. If one instead assumes a charge particle rapidity distribution peaked at target and projectile rapidities, (i.e. the initial charge distributions of the colliding nuclei) then one finds that the electric potential is suppressed by a factor $\gamma_{cms}^2 \sim 100$ near midrapidities at SPS energies as compared to the constant

[†]The exact expression is obtained by replacing the time $t$ in (9) by $\sqrt{v_0^2 t^2 + r_\perp^2(1-v_0^2)}$, where $v_0$ is the lower or upper velocity. Here, $v_0 < c$ limits the longitudinal extent of the charge cylinder and thus removes the $t = 0$ singularity for nonvanishing $\mathbf{r}_\perp$. Since the times and distances relevant for Coulomb effects are $t \simeq R/c$ and $r_\perp \sim R$ respectively, where $R$ is the size of the nuclei, we can safely approximate $v_0 \simeq c = 1$.

rapidity distribution. In contrast, assuming a static central charge the push given to the positively charged pions is greatly overestimated.

As above we assume that the pions are trapped in the hot matter until freeze-out at time $\tau_f$. After this time the pions can propagate freely only influenced by the Coulomb field. During the collision the particle rapidity distributions change due to interactions. However, at late times the retarded potential (7) arises mainly from the free streaming phase or the flowing phase in the period between the collision and freeze-out. According to Gauss law the electric field in the interior is reduced by an area factor $r_\perp^2/R_f^2$, where $R_f$ now is the transverse size of the system at freeze-out, i.e.,

$$\mathbf{E}(\mathbf{r}_\perp, t) = e\frac{dN^{ch}}{dy}\frac{2}{t} \times \left\{ \begin{array}{l} \frac{\mathbf{r}_\perp}{R_f^2}\,, \;\; r_\perp < R_f \\ \frac{\mathbf{r}_\perp}{r_\perp^2}\,, \;\; r_\perp > R_f \end{array} \right\}. \tag{10}$$

A charged pion of transverse momentum $p_{\perp,0}$ at freeze-out and final momentum $p_\perp$ receives a momentum change or "Coulomb kick"

$$\Delta\mathbf{p}_\perp = \mathbf{p}_\perp - \mathbf{p}_{\perp,0} = \pm e\int_{\tau_f}^{\infty} \mathbf{E}(r_\perp, t)dt\,, \tag{11}$$

where the $\pm$ refers to positive and negative pions, respectively. If the Coulomb kick is small so that the pion velocity changes little, the position of a $\pi^\pm$ at freeze-out $\mathbf{r}_f$ with velocity $\mathbf{v}_\pi$ developes according to

$$\mathbf{r} = \mathbf{r}_f + \mathbf{v}_\pi(t - \tau_f)\,. \tag{12}$$

For an ensemble of pions we obtain the momentum change by averaging over the freeze-out position $\mathbf{r_f}$ in Eq. (11). The result will generally depend on both $R_f$ and $\tau_f v_\perp$. We find, however, that the momentum change is only a slowly decreasing function of the freeze-out time. For a freeze-out time of $\tau_f = 8$fm/c, $R_f \sim 10$fm and with pion velocities as given by the low $m_\perp$ data, we obtain the estimate

$$p_c \equiv |\Delta p_\perp| \simeq 2e^2\frac{dN^{ch}}{dy}\frac{1}{R_f}\,, \tag{13}$$

in the direction of $\pm\mathbf{p}_\perp$. The variation with freeze-out time is $\pm 10\%$ for $v_\perp\tau_f/R_f$ in the range $0.5 - 0.8$.

It is important to note that the difference between results for the static charge of Eqs. (2,3) and the rapidly expanding charge of Eqs. (11,13). In the former case the field decreases at large distances as $r^{-2}$ whereas in the latter it decreases as $t^{-1}r_\perp^{-1}$. As a consequence, the *energy* is shifted by an amount proportional to the charge $Z$ in the former case while in the latter the *momentum* is shifted by an amount proportional to $dN^{ch}/dy$. In both cases, however, the scale of the shifts is determined by the source size $R_f$ at freeze-out.

As above we can derive the Coulomb effect on the transverse particle distribution functions

$$\frac{dN}{d^2p_\perp} = \frac{dN_0}{d^2p_{0,\perp}}\,\frac{p_{0,\perp}}{p_\perp}\,. \tag{14}$$

The pion spectra are well reproduced by $dN/d^2p_\perp \propto \exp(-m_\perp/T)$ with $T \simeq 150$ MeV at both AGS and SPS energies [18]. Defining $m_\perp^\pm = \sqrt{m^2 + (p_\perp \pm p_c)^2}$ and using Eqs. (11) and (13)

$$\frac{\pi^-}{\pi^+} \equiv \frac{dN^-/d^2p_\perp}{dN^+/d^2p_\perp} = \langle\frac{\pi^-}{\pi^+}\rangle \exp\left(\frac{m_\perp^- - m_\perp^+}{T}\right)\frac{p_\perp + p_c}{p_\perp - p_c}\,. \tag{15}$$

The pion ratio predicted by (15) is compared to AGS and SPS data in Figs. 3 and 4. Here the experimental values $\langle \pi^-/\pi^+ \rangle \simeq 1.2$ and 1.05 at AGS [19] and SPS [20] energies, respectively, have been used. These values are closer to unity than at SIS energies due to the abundant pion production not connected to $\Delta$-resonances. The experimental data is well reproduced with $\Delta p_\perp^{AGS} \simeq 20$ MeV/c and $\Delta p_\perp^{SPS} \simeq 12$ MeV/c. From the measured proton rapidity distribution, $dN^p_{AGS}/dy \simeq 70$ and $dN^p_{SPS}/dy \simeq 37$, and Eq.(13) we can now extract the size of the systems at freeze-out: $R_f^{AGS} \simeq 10$ fm and $R_f^{SPS} \simeq 9$ fm. The sizes are substantially larger than the geometrical radii $R_{geom} \simeq 6 \sim R_{Pb}$ fm of the collision zones (for 14% centrality) indicating that significant expansion takes place before freeze-out.

For the $S+S$ collision at the SPS $dN^p/dy \simeq 4$. Assuming $R_f \simeq 4$ fm we find a rather small value for $p_c \simeq 4$MeV/c, and the corresponding Coulomb effect is thus very small as seen in Fig. 9.

## IV. SLOW PARTICLES

Slow pions, i.e. pions with velocities $v_\pi$ smaller than the expansion velocity of the net charge which is typically given by the proton velocities $v_p$, are less affected by the Coulomb field. According to Eq. (1) such slow pions should have kinetic energies below 20 MeV at SIS energies and transverse kinetic energies below 40 MeV at SPS energies.

We can estimate the effect of expansion by simply assuming that the protons solely determine the expansion of the charge. If we assume that the proton velocities are distributed according to a nonrelativistic Boltzmann distribution with temperature $T_p$, the charge should therefore be reduced by a factor

$$\mathcal{R}_n^{exp} = \frac{\int_0^{v_\pi} \exp(-\frac{1}{2} m_p v^2/T_p)\; v^{n-1} dv}{\int_0^{\infty} \exp(-\frac{1}{2} m_p v^2/T_p)\; v^{n-1} dv} \;=\; \left\{ \begin{array}{ll} 1 \,-\, \exp(-x^2), & n=2 \\ erf(x) - (2/\sqrt{\pi}) x\, \exp(-x^2), & n=3 \end{array} \right\}, \tag{16}$$

where $x = \sqrt{\frac{1}{2} m_p v_\pi^2/T_p}$ and $erf(x)$ is the error function. The exponent $n = 2$ is for cylindrical geometry with transverse expansion and $n = 3$ is for spherical expansion. Reducing the charge (or proton rapidity density) by this factor reduces the Coulomb kick $V_c$ (or $p_c$) is diminished by an amount which now depends on the particle energy. This fact needs to be properly included in the Jacobian $dp_{0,\perp}/dp_\perp$ of the resulting charge particle distribution (Eq. (14)) The result of transverse expansion is shown in Fig. 5 for $\pi^-/\pi^+$ with $p_c = 15$ MeV/c and in Fig. 6 for $K^-/K^+$.

The factor (16) overcorrects for transverse expansion since it completely removes the Coulomb corrections for $v_\pi = 0$. However, even for $v_\pi = 0$ the pions are still accelerated by the Coulomb field which decreases as $t^{-1}$. We therefore consider slow pions embedded in a charge expanding with velocity $v_p$. Pions with velocities smaller than $v_p$ stay inside the expanding source in the potential decreasing with time. As the net positive charge $Z$ or $2dN^p/dy$ expands spherically or transversely with velocity $v_p$, the radius increases with time

$$R = R_f + v_p(t - \tau_f)\,. \tag{17}$$

Here, $R_f$ is the radius at freeze-out radius at freeze-out time $\tau_f$. The pion moves according to Eq. (12) and we will find that the Coulomb effect leads only to minor changes in pion momenta, hence to leading order we can assume that $\mathbf{v}_\pi$ is constant.

In the case where pions move slowly in the electric field

$$\mathbf{E}(t) = Ze\frac{\mathbf{r}}{R^3}\,. \tag{18}$$

of a sphere with a constant charge density the net momentum change is

$$\Delta\mathbf{p} = \pm e \int_{\tau_f}^{\infty} \mathbf{E}(t)\, dt = \pm \frac{Ze^2}{2R_f v_p} \left[ \frac{\mathbf{v}_\pi}{v_p} + \frac{\mathbf{r}_f}{R_f} \right] , \tag{19}$$

for positive and negative pions, respectively. Retardation effects are ignored for simplicity which is a rather good approximation for spherical systems where the charge moves primarily in radial direction (see also appendix A). The average of the freeze-out position vanishes, $\langle \mathbf{r}_f \rangle = 0$, if there is no transverse flow. Therefore, averaging over $\mathbf{r}_f$ will to first approximation only lead to a smearing of the $\pi^+$ and $\pi^-$ distributions and by the *same* amount. When taking ratios this effect cancel out, and we therefore ignore it in the following. The final momentum is thus

$$\mathbf{p} = \mathbf{p}_0(1 \pm C_3) , \quad C_3 = \frac{Ze^2}{2m_\pi v_p^2 R_f} , \tag{20}$$

i.e., the positive and negative pion momenta are scaled up and down respectively.

The case of rapid longitudinal expansion was studied in the previous section. The resulting electric field is given by Eq. (10) and from Eq. (19) we find the change in transverse momentum

$$\Delta\mathbf{p}_\perp = \mathbf{p}_\perp - \mathbf{p}_{\perp,0} = \pm e \int_{\tau_f}^{\infty} \mathbf{E}(r_\perp, t) dt \simeq \pm e^2 \frac{dN^{ch}}{dy} \frac{2}{R_f} \frac{\mathbf{v}_\perp}{v_p} . \tag{21}$$

The latter approximate expression holds under the condition $v_p \tau_f \lesssim R_f$. For small $p_\perp$ we can approximate $p_\perp = m v_\perp$ and thus find

$$\mathbf{p}_\perp = \mathbf{p}_{\perp,0}(1 \pm C_2) \quad ; \quad C_2 \simeq e^2 \frac{dN^{ch}}{dy} \frac{2}{m v_p R_f} . \tag{22}$$

The Coulomb effect on particle distribution functions can be obtained from particle conservation, i.e. $dN = dN_0$ is the same for initial and final pions,

$$\frac{dN}{d^n p} = \frac{dN^0}{d^n p_0} (1 \pm C_n)^{-n} . \tag{23}$$

The ratio of negative to positive pions is then

$$\frac{\pi^-}{\pi^+} \equiv \frac{dN^-/d^n p}{dN^+/d^n p} = \langle \frac{\pi^-}{\pi^+} \rangle \left( \frac{1 + C_n}{1 - C_n} \right)^n \exp\left( \frac{E^- - E^+}{T} \right) , \tag{24}$$

where $E^\pm = \sqrt{m^2 + p^2(1 \pm C_n)^2}$. Notice that $C_n \ll 1$ is implicitly required since we approximated the trajectory $\mathbf{r}(t)$ by assuming constant velocity in the electric field.

Introducing the kinetic energy $E_{kin} = E - m$ (for $n = 3$) and $E_{kin} = m_\perp - m$ (for $n = 2$), the ratio decreases linearly as

$$\frac{\pi^-}{\pi^+} \simeq \langle \frac{\pi^-}{\pi^+} \rangle \left( 1 + 2nC_n (1 - \frac{E_{kin}}{T}) \right) . \tag{25}$$

for small kinetic energies, $E_{kin} \ll m$. The ratio is thus enhanced by $2nC$ at small $m_\perp$ and decreases linearly on a scale determined by $T$.

It is interesting to compare our approximation with the exact analytic result found by Ayala and Kapusta [21] treating the motion of nonrelativistically positively charged particles in a Coulomb field from a homogeneously charged expanding sphere. With their parameters ($Z$=158, $R_f$ = 8 fm, $v_p$=0.2) we obtain $C_3 = 0.7$ for kaons. This leads to

a reduction of low momentum $K^+$ by a factor $(1+C_3)^{-3} = 0.2$ similar to their value of 0.15 determined from Fig. 3a in [21]. However one should be aware that the suppression factors behave asymptotically differently in the limit $v_p \to 0$.

Next we estimate the crucial parameters $C_2$ and $C_3$. In central $Au + Au$ collisions at SIS energies the proton velocity can be estimated from the slope of proton spectra $v_p^2 \simeq 3T_p/m_p \simeq 0.3$. With a central charge of $Z = 122$ (15% centrality) we obtain $C_3 \simeq 0.3$ that according to (24) leads to a large enhancement by a factor $\sim 6$ at zero momentum. Unfortunately, at SIS energies no measurements are available at very low pion energy. For SPS we assume cylindrical geometry $n = 2$. Consequently, going from $C_3$ to $C_2$ we replace $Z$ by $2dN^p/dy$. With $v_p^2 \simeq 2T_p/m_p \simeq 0.6$ we obtain $C_2$ =0.12 and find a $\pi^-/\pi^+$ ratio (24) of 1.8 in agreement to the data.

As mentioned the derivation applies not only to pions but to all particles, for example, kaons. As the kaon is heavier we expect from (22) that the Coulomb enhancement of the $K^-/K^+$ ratio is smaller by a factor of $m_\pi/m_K \sim 1/3$.

Experiments at the AGS [4] and SPS [18] indicate that transverse flow is important in collisions with very heavy nuclei. Transverse flow decreases the $m_\perp$ slopes observed in $m_\perp$ spectra of pions, kaons and protons. The measured "effective temperatures" are thus larger than the intrinsic temperatures. In our analysis transverse flow has several effects. The temperature employed in the Boltzmann spectrum should not be the effective slope parameter, $T \simeq 200$ MeV but the intrinsic temperature, $T \simeq 140$ MeV. Furthermore, flow leads to larger $v_p$ and nonvanishing $\langle \mathbf{r}_f \rangle$ in (19). Particles with transverse momentum $\mathbf{p}_\perp$ from a thermal source of temperature $T$ with transverse flow $ur_\perp/R_f$ arrive on average from a point displaced from the center by $\langle \mathbf{r}_f \rangle = \mathbf{p}_\perp u R/2T$. Transverse flow thus adds a term to (19) for charged pions and usually reduces $C_n$.

We can summarize the discussion of Coulomb effects by addressing the important scales entering. In the spherically symmetric case (n=3) the Coulomb kick is given by $V_c \simeq \pm Ze^2/R_f$. For slow expansion the particle kinetic energies are *shifted* (see Eq. (3)) by this amount, i.e., the relevant dimensionless quantity is $V_c/m_\pi v_\pi^2$ instead. For rapid expansion $v_p \gg v_\pi$ the kinetic energies are instead *scaled* (see Eq. (20) by an amount proportional to $V_c/m_\pi v_p^2$. In the dimensionless quantity $v_\pi^2$ is replaced by $v_p^2$ simply because it is the fastest particle velocity that matters. A similar behavior is found for the cylindrical expansion (n=2) except that in this case the relevant quantity is the *momentum* instead of *kinetic energy* due to the rapid longitudinal expansion and the Coulomb kick is $V_c \simeq (e^2/R_f)dN^p/dy$. For slow expansion the momentum is shifted by $V_c$ (see Eq. (13) and the corresponding dimensionless parameter is $V_c/m_\pi v_\pi$. For an expansion faster than the pion velocity the momenta are scaled by an amount proportional to $V_c/m_\pi v_p$ (see Eq. (22)). Again the pion velocity is replaced by the proton velocity since the fastest particles determine the magnitude of the Coulomb effect.

## V. DYNAMICAL MODEL

After the previous discussion of the typical properties of the Coulomb effect in different energy regions we apply a more detailed model [10] which allows finer details of the freeze-out scenario. Inspired by the Bjorken picture of approximate boost invariance we assume a cylindrical geometry and include both longitudinal and transverse flow. We introduce the following parameters: the width $\Delta y_{ch}$ of the rapidity distribution of the charge (usually a Gaussian

distribution is taken), the thermal equilibrium temperature $T$, the mean transverse flow velocity $\langle\beta\rangle$, the source radius $R_f$, and the freeze-out time $\tau_f$. The initial charge distribution at freeze-out is assumed to follow a Boltzmann distribution which includes the different chemical potentials for positively and negatively charged particles. Further details are explained in ref. [10].

After freeze-out the different species of particles, mainly nucleons, pions, and kaons, are assumed to move freely. Their momentum distribution is given by a thermal distribution superimposed on a hydrodynamic flow. The influence of the electromagnetic forces on the emitted particles will increase the initial charge asymmetry. This influence is treated as a first order perturbation, assuming that the electromagnetic field is generated by the charged particles moving with their unperturbed initial velocities. This method is justified as long as the electromagnetic potential is small compared to the mean kinetic energy of the particles.

To calculate the electromagnetic potential $A^\mu$ at the space-time $x^\mu = (t, \mathbf{r})$

$$A^\mu(t, \mathbf{r}) = \int d\mathbf{r}' \frac{j^\mu(t - |\mathbf{r} - \mathbf{r}'|, \mathbf{r})}{|\mathbf{r} - \mathbf{r}'|} \,, \tag{26}$$

the knowledge of the currents $j^\mu(t, \mathbf{r})$ during the whole collision history is needed. Retardation effects are essential, especially at ultra-relativistic energies where the longitudinal motion is not fully decelerated. To describe the situation before freeze-out we have in ref. [10] used a simple hydrodynamical scenario to describe the situation before freeze-out. We assume a linearly increasing longitudinal and transverse flow of the matter between the overlap time $t = 0$ and the freeze-out time $t = \tau_f$, i.e., the radius at freeze-out is $R_f = R_{geom} + 0.5\tau_f\beta_S$, where $R_{geom}$ is the initial or geometrical radius of the overlap zone at the collision time and $\beta_S$ the velocity at the surface of the source. The linear motion of the particles allows one to calculate the net Coulomb mean field as a superposition of the electromagnetic fields of the individual charged particles. If the particles denoted by $i$ with charge $q_i$, mass $m_i$, and four-velocity $u_i^\mu = (1, \mathbf{v})/\sqrt{1 - \mathbf{v}^2}$ start at space-time $y_i^\mu$ we get

$$A^\mu(x^\mu) = \sum_i q_i \frac{u_i^\mu}{\sqrt{[(u_i)_\nu(x^\nu - y_i^\nu)]^2 - (x^\nu - y_i^\nu)^2}}. \tag{27}$$

Since the calculations of retardation are very cumbersome we also discuss approximations in appendix A.

The motion of the particles is treated relativistically in the potential (27)

$$m_i \frac{d}{d\tau_f} u_i^\mu = q_i \, u_i^\nu \left( \frac{\partial A_\nu}{\partial x_\mu} - \frac{\partial A^\mu}{\partial x^\nu} \right) \,, \tag{28}$$

where $\tau_f$ denotes the proper time of the particle. The $\pi^-$ and $\pi^+$ spectra are finally calculated by a sampling the final momenta over a set of solutions obtained with different initial conditions obtained from the freeze-out parametrization.

In Figs. 7-9 we show the calculations for the three above mentioned experiments. We concentrate on the sensitivity to variations of the freeze-out time. The flow velocity and temperature were determined from fits to the $m_\perp$ slope of available spectra for particles with different masses, see refs. [11,18,19]. For a systematic overview we refer to ref. [22].

Fig. 7 shows the result for SIS energies which has to be compared to the schematic model of Fig. 1. For a temperature of 75 MeV and mean transverse velocity of $\langle\beta\rangle = 0.3$ corresponding to a surface velocity of $\beta_s$ =0.5 good agreement to the data is obtained. This gives a freeze-out radius of $R_f = 6fm + 0.5\tau_f\beta_s$= 8 fm leading to a break-up density of 0.8 $\rho_0$. This value is just the same as that obtained in section II, but larger than the value obtained in the

transport model [13]. The final production time in that model is rather long $\sim 25$ fm/c which is partially due to long lived $\Delta$ resonances.

Figs. 8 and 9 address the ultra-relativistic regime. Here, the measured widths of the particle rapidity distributions, $\Delta y_{ch}$, is about 0.7 and 1.3 for AGS and SPS energies respectively. A mean flow velocity of $\langle\beta\rangle$ =0.42 or $\beta_s = 0.62$ was used together with a moderate temperature of 140 MeV and 120 MeV, respectively. The results at AGS energies are relatively insensitive to the freeze-out time since the charge diffuses slower in the longitudinal direction than for SPS energies. A freeze-out time of 10 fm/c seems to be compatible with the data, while for SPS energies a time of about 7 fm/c is required. We also show the relatively modest enhancement for the reaction of $S$ on $S$ at SPS energies, where the rapidity density of the charge is slightly depleted at midrapidity. For a more detailed discussion at SPS energies we refer to ref. [10].

## VI. COMPARISON TO HBT ANALYSES

The source for pions, kaons and other particles created in high energy nuclear collisions at freeze-out is also studied in two-particle correlation functions. Such Hanbury-Brown and Twiss (HBT) analysis provides complementary information on freeze-out time and source size. Pion correlation functions are, however, affected by resonance decays which actually produce the majority of the pions. Resonances lead to an increase of the measured HBT radii, effective source sizes and life-times [23,24]. A significant fraction $f$ of the pions stem from *long lived resonances* in ultrarelativistic collisions which reduces the correlation function by a factor $\lambda^{\pi\pi} \sim (1-f)^2$. Experimentally, $\lambda^{\pi\pi} \simeq 0.5 - 0.6$ [25] and so $f \simeq 25\%$. Also, long lived resonances reduce the Coulomb effect by a minor amount as discussed below. Though these and other effects as Coulomb corrections, detector cuts, etc., are important for a detailed analysis, we will ignore them for our qualitative comparison.

The transverse HBT radii are usually referred to as the outward and sideward radii in the direction along and perpendicular to the transverse momentum of the two correlated pions, respectively. The outward HBT radius contains a number of fluctuations as duration of emission and resonances life-times and are furthermore affected by opacities and moving emission surfaces [26]. The sideward HBT radius $R_s$ is more directly connected to the geometric size of the source at freeze-out. For a source of constant pion density the sharp cut-of radius is given by $R_f = 2R_s$, and with $R_s \simeq 5$ fm [25] in central $Pb + Pb$ collisions at 160 A·GeV we obtain $R_f \simeq 10$ fm. This number is larger than the geometrical radius of a $Pb$ nucleus indicating that expansion takes place before freeze-out.

In a longitudinally expanding system with Bjorken scaling the freeze-out time is related to the longitudinal HBT radius by $\tau_f = R_l \sqrt{m_\perp/T}$. From the NA44 data $R_l \simeq 5.5$ fm [25] we estimate $\tau_f \simeq 8$ fm/c. For comparison RQMD calculations predict substantially larger values for the freeze-out time, $\tau_f$=15 fm/c [27]. Assuming that the source starts out with the mean geometrical radius $R_{geom} = 6$fm (for the 15% centrality) at the collision and develops transverse flow $\beta_s$ up to freeze-out, we find a radius of $R_f = R_{geom} + \beta_s \tau_f/2 \simeq 9$ fm, which is slightly smaller than the freeze-out radius obtain from the sideward HBT radius. We conclude that both freeze-out times extracted from the longitudinal and transverse HBT radii are compatible at SPS energies with the one we find from $\pi^-/\pi^+$ data. The Coulomb freeze-out radius is also comparable to the HBT radii found at AGS energies as seen from Fig. 10. At SIS energies we extract the HBT radius from the average of the $\pi^+\pi^+$ and $\pi^-\pi^-$ HBT radii [29] by multiplying by

the geometrical factor, $R_f = \sqrt{5/3}R_{rms} \simeq 15$fm. This radius is considerably larger than the one extracted from the Coulomb effects.

## VII. RESONANCE DECAY

In ultrarelativistic collisions resonance decay into pions is important. If pions stem from resonances with a life time larger than the freeze-out time, their Coulomb push is reduced. This is important for the long lived resonances $\omega, \eta, \eta', K^0_S$, etc.. As mentioned above they amount to roughly $f = 25\%$ if the reduction of the HBT correlation function is solely caused by long lived resonances. If a fraction $f$ is unaffected by the Coulomb field only the fraction $(1-f)$ of the distribution function in Eq. (14) should be transformed. The resulting $\pi^-/\pi^+$ ratio is therefore

$$\frac{\pi^-}{\pi^+} = \langle\frac{\pi^-}{\pi^+}\rangle \frac{(1-f)\frac{p_\perp+p_c}{p_\perp}e^{-m_\perp^+/T} + fe^{-m_\perp/T}}{(1-f)\frac{p_\perp-p_c}{p_\perp}e^{-m_\perp^-/T} + fe^{-m_\perp/T}}\,. \tag{29}$$

The effect of long lived resonances are shown in Fig. 5 for $f = 0.25$ and $p_c = 15$ MeV/c. As they reduce the Coulomb effect, the best fit is now obtained for a slighly larger value of $p_c = 15$ MeV/c. If the long lived resonances produce pions at different $p_\perp$ one should use a different effective $m_\perp$ slope for those in (29).

Resonances may decay differently into $\pi^-$ and $\pi^+$ depending on pion momenta and thus provide another mechanism for changing pion distributions at low $p_\perp$. This is the case for $\Lambda$ and $\bar{\Lambda}$ particles. In central $Pb+Pb$ collision at SPS energies the number of $\Lambda$'s produced per unit rapidity at central rapidies is $dN^{\Lambda-\bar{\Lambda}}/dy = 19 \pm 7$ [15]. Of these 64% decay into $\pi^-$. Compared to $dN^{\pi^-}/dy = 160 \pm 10$ the $\Lambda$'s thus contribute $\sim 8\%$ to the $\pi^-$ yield. Since the decay energy of pions amounts to only 35 MeV in the $\Lambda$ rest frame they would lead to an enhancement of the $\pi^-/\pi^+$ ratio of $\sim 1.4$ if included. The ratio would fall off slowly as a function of the transverse momentum. However, only at most a few percent of those pions can enter the detector in the NA44 measurements because the $\Lambda$'s travel $\sim 60$cm before decaying due to the long life time. Therefore they do not contribute to the measured $\pi^-$ yield. Both the $Pb+Pb$ data and the $S+S$ data are compatible with the Coulomb effect but cannot be explained by resonances alone. The same conclusion was drawn from RQMD analyses [16].

## VIII. THE $K^-/K^+$ RATIO

The $K^-/K^+$ ratio provides another way to test the Coulomb effect and obtain information on freeze-out. We estimate $\Delta p_\perp$ by taking the best fit to the $\pi^-/\pi^+$ data, however, correcting it for the slightly smaller HBT radii for kaons than pions. We estimate $\Delta p_\perp \sim 15$ MeV/c. Furthermore we take the kaon temperature of $T_K = 230$ MeV from [18] and $\langle K^+/K^-\rangle = 0.68$ from [30]. We can then predict the $K^-/K^+$ as shown in Fig. 6. As the kaons are heavier than the pions their kinetic energies are less affected by the momentum change. Also, the kaons move slower and are more affected by transverse expansion of the net (proton) charge (see appendix A). A smaller number of protons remains to give the kaons a Coulomb kick and the $K^-/K^+$ ratio is closer to unity as seen in Fig. 6.

HBT analyses show that the kaon correlation function is not reduced by long lived resonances, since $\lambda^{KK} \simeq 1$. On the other hand, the absorption of $K^-$ on nucleons by $K^-N \to \Lambda\pi$ is much larger than for $K^+$. Therefore the initial ratio $K^-/K^+$ may differ in very heavy ion collisions from light ones since the stopping is larger. The measured

$K^-$ spectrum [33] in fact shows a decrease at low $p_\perp$ in heavy ion collisions as compared to light ones by almost a factor of two. Thus, the resulting $K^-/K^+$ ratio could be even an increasing function of the transverse energy. Recent NA44 measurements do not show a significant dependence on the transverse energy. If the enhancement of the $K^-/K^+$ ratio predicted in Fig. 6 should exceed the measured one, this would indicate new physics.

Kaons may also experience a strong interaction with the mean field from hadrons. Early reports on low $p_\perp$ enhancement for $K^+$ at AGS energies - referred to as "cold kaons" - led to suggestions of a strong attractive potential [34] that dominated the repulsive Coulomb potential. The cold kaons have, however, not been confirmed in later AGS experiments. In nuclear matter the $K^+$ interaction is repulsive [35] but one cannot rule out that it becomes attractive in hot and dense matter.

## IX. SUMMARY

Coulomb effects are very sensitive to the expansion dynamics of high energy nuclear collisions. At lower energies the expansion of the charge cloud, which consists mainly of protons, is slow compared to typical pion velocities. The pions experience the full Coulomb kick and the $\pi^-/\pi^+$ ratio becomes large at small pion momenta as described in Eq. (5). At higher collision energies the expansion of nucleons is faster and exceeds that of the very slow pions. The Coulomb field, which the pions feel, vanishes rapidly within the typical expansion time. The resulting $\pi^-/\pi^+$ ratio is only enhanced by $\sim 60\%$ at the smallest measured transverse momentum $p_\perp$ at AGS and SPS energies and can be approximately described by Eq. (15). At ultrarelativistic energies the rapid longitudinal expansion and retardation of electromagnetic fields are important and the charge rapidity density replaces the central charge. The Coulomb field affects small pion transverse momenta on a scale given by the total Coulomb energy. The Coulomb effect on kaons is smaller than for pions due to their larger mass.

The Coulomb effect provides information on the sources produced in relativistic heavy ion collisions at freeze-out independent of HBT analyses and flow studies in particle spectra. HBT methods analyse the source at freeze-out, and Coulomb effects occur after freeze-out. The measured enhancement of the $\pi^-/\pi^+$ ratio provides a severe constraint on the values found by various methods. From the investigations presented here the source sizes and freeze-out times obtained from HBT analyses seem to be compatible with those obtained from Coulomb effects. Calculations using transport models like BUU or RQMD tend to find larger freeze-out times indicating the need for a consistent description of the whole process to calculate charge asymmetry and HBT correlations.

At RHIC and LHC energies smaller stopping is expected than at SPS and AGS energies, and the charge density $dN^p/dy$ will be smaller at midrapidity but larger near target and projectile rapidities. Given the amount of stopping we can try to predict the resulting $\pi^-/\pi^+$ ratios at RHIC and LHC. The total $\langle\pi^-/\pi^+\rangle$ production should be very close to unity due to the abundant pion production. The transverse size of the system at freeze-out can be estimated from the HBT radii assuming that the radii continue to increase slowly with collision energy as is found experimentally up to energies 160A·GeV. By extrapolating we estimate $R \simeq 15$ fm. If we, for example, assume $dN^p/dy = 25$ we find $p_c = 5$ MeV/c. The resulting $\pi^-/\pi^+$ ratio is shown in Fig. 4 (not corrected for resonances and transverse proton expansion). However, if a phase transition to a quark-gluon plasma occurs, these predictions may change drastically. The freeze-out may occur much later so that the source is more longitudinally and transversely expanded leading to

a reduced Coulomb effect.

We acknowledge very informative discussions with A. Hansen and Nu Xu from the NA44 collaboration. Support from The Danish Natural Science Research Council is appreciated.

## APPENDIX A: Effects of Retardation

In ref. [13] approximations were applied by using the Coulomb potential $\phi$ as the only part of the four-potential. This potential $\phi$ is calculated as being $A^0$ of (26), but neglecting the retardation. Thus, the equation of motion simplifies to

$$m_i \frac{d}{d\tau} u^k = u^0 \, q_i \frac{\partial \phi}{\partial x^k}, \quad k = 1, 2, 3. \tag{30}$$

We demonstrate the deviations one obtains when applying the approximative method (30) where retardation and the spatial components are neglected.

At moderate energies where the thermal velocities of the nucleons are not large this approximations works well. In Fig. 11 we show the effect on the $\pi^-/\pi^+$ ratio in the transverse direction kinetic energy for a reaction of gold on gold nuclei. As an example we use the following parameters: $\Delta y_{ch} = 0.4$, $T = 75$ MeV, $\langle\beta\rangle = 0.3$, and $\tau_f = 7$ fm/c which give in Fig. 7 reasonable agreement with the data. One recognizes that the approximate treatment (30) is well applicable and leads roughly to a 10% underestimation of the ratio at an lab-angle of $44^o$ which corresponds nearly to the transverse direction in the c.m. system.

Larger effects are expected at ultrarelativistic energies. In Fig. 12 we show the calculated charge ratio at small momentum as a function of rapidity for a lead on lead collisions at 158 A·GeV. The solid line is calculated using Eq. (28) and shows a $\pi^-/\pi^+$ ratio at zero transverse momentum which follows nicely the rapidity distribution of the net charge as it is expected from our considerations in section III. The approximate method shows quite a different behavior with a maximum off-midrapidity. This is because the potential $\phi$ is not able to cope with the translational invariance which is hidden in the correct potential (26). Since the calculation is carried out in the cm-system it fails completely for larger rapidities. In the correct treatment the action of the component $A^0$ is compensated by the longitudinal part of the magnetic field. The dotted curve shows the result if one treats the Coulomb potential as a genuine scalar potential which means dropping the term $u^0$ on the right hand side of Eq. (30). This method is quite an insufficient approximation which even is not applicable for small energies as can be seen in Fig. 11.

---

[1] W. Benenson et al., Phys. Rev. Lett. **43**, 683 (1979);
K. G. Libbrecht and S.E. Koonin, Phys. Rev. Lett. **43**, 1581 (1979)

[2] A. Wagner et al., preprint Th Darmstadt, IKDA 95/9 (1995) and submitted to Phys. Lett.

[3] D. Pelte et al., Z.Phys.**A357** (1997) 215

[4] L. Ahle et al., Nucl. Phys. **A610** (1996) 139c

[5] H. Bøggild et al., NA44 collaboration, Phys. Lett. **B 372**, 343 (1996)

[6] M. Gyulassy and S.K. Kauffmann, Nucl. Phys. **A362** 503 (1981)

[7] R. Stock, Phys. Rep. **135** (1986) 259.

[8] Bao An Li, Phys. Lett. **B346** (1995) 5.

[9] T.Osada, S. Sano, M. Bijyajima and G. Wilk, Phys. Rev. **C54** (1996) 54; hep-ph/9702347

[10] H.W. Barz et al., Phys. Rev. **C56** (1997) 1553

[11] C. Müntz et al., Z. Phys. **A357** (1997) 399

[12] G. Baym and P. Braun-Munzinger, *Nucl. Phys.* A 610 (1996) 286c.

[13] S. Teis et al., Z. Phys. **A356** (1997) 421

[14] J. D. Jackson, "Classical Electrodynamics", NY, Wiley & Sons,1963.

[15] S.V. Afanasev, NA49 collaboration, Nucl. Phys. A610, 76c (1996)

[16] I. G. Bearden et al., NA44 collaboration, Phys. Lett. **B388**, 431 (1996); Nu Xu et al. (NA44), Nucl. Phys. **A610**, 175c (1996)

[17] J.D. Bjorken, Phys. Rev. **D27**, 140 (1983)

[18] I.G. Bearden et al., NA44 collaboration, Phys. Rev. Lett. **78**, 2080 (1997).

[19] P. B. Braun-Munzinger et al., Phys. Lett. **B 344**, 43 (1995)

[20] P. Jones, NA49 collaboration, Nucl. Phys. **A610** (1996) 188c.

[21] A. Ayala and J. Kapusta, Phys. Rev. **C56** (1997) 407.

[22] N. Herrmann et al. (FOPI collab.), Nucl. Phys. A610, 49c (1996).

[23] H. Heiselberg, *Phys. Lett.* **B379** (1996) 27.

[24] U.A. Wiedemann, U. Heinz, nucl-th/9611031.

[25] I.G. Bearden et al., NA44 collaboration, Nucl. Phys. **A610** (1996) 240c.

[26] H. Heiselberg and A. Vischer, Z. Physik **C** (1997) in press; Phys. Lett. **B** (1997) in press.

[27] H. Sorge et al., Phys. Lett. **B373**, 16(1996).

[28] D. Pelte, FOPI collaboration, proc. of Int. Conf. $4\pi$ detector systems, Poiana Brasov, 1996, Rumania.

[29] J. Barrette et al., E877 collaboration, Nucl. Phys. **A610** (1996) 227c.

[30] M. Murray et al., NA44 collaboration, Heavy Ion Physics **4** (1996) 213.

[31] K. Kadija et al., NA49 collaboration, **A610** (1996) 248c.

[32] L. Rosselet et al., WA98 collaboration, **A610** (1996) 256c.

[33] H. Böggild et al., NA44 collaboration, *Z. Phys.* **C69**, 621 (1996); and preliminary results presented at "Quark Matter 1997", Tsukuba, Japan.

[34] V. Koch, Nucl. Phys. **A591**, 531c (1995).

[35] see, e.g., W. Weise, Nucl. Phys. **A610** (1996) 35c.

[36] P. Braun-Munzinger et al., Phys. Lett. **B 365**, 1 (1996)

**Figure captions**

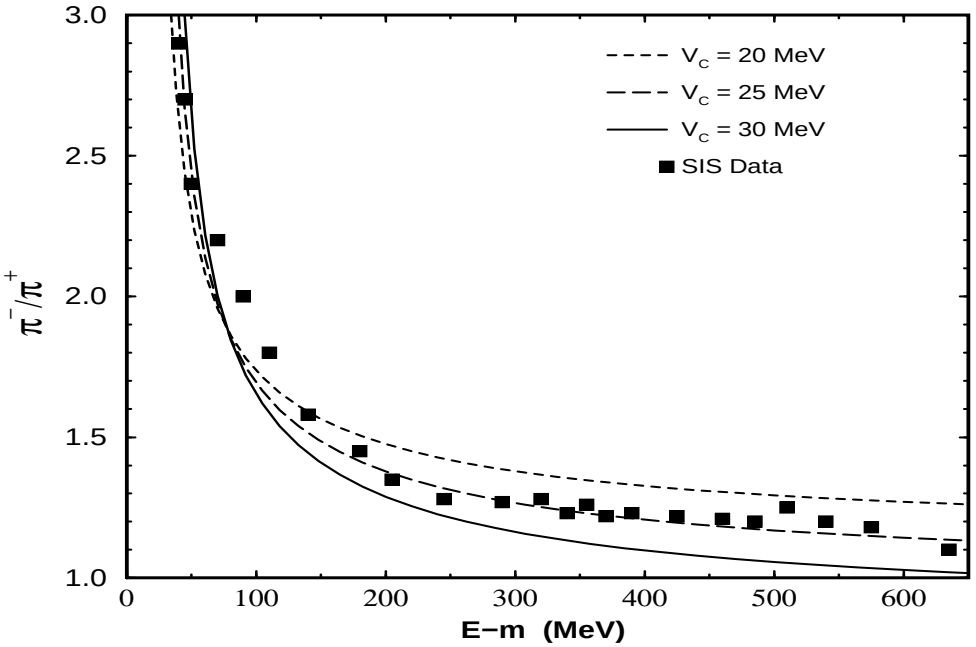


FIG. 1. Experimental $\pi^-/\pi^+$ ratios [2] for the reactions $Au + Au$ at 1.0 AGeV as a function of the pion kinetic energy around 44 degrees from forward direction in the lab system (corresponding to ca. 90 degrees in cms). Curves show calculations according to Eq. (5) for the case of a slow expanding spherical source using various Coulomb energies $V_c$. Using a slope parameter of 75 MeV a value of $V_c \simeq 27$ MeV gives good agreement with data (full squares) [2].

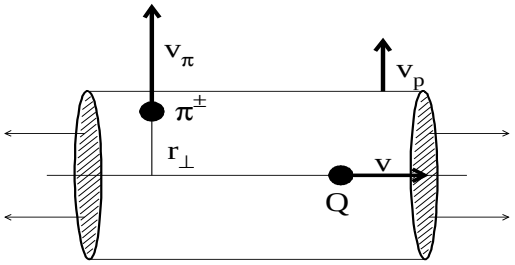


FIG. 2. Sketch of the ultrarelativistic collision where the pion at the transverse distance $\mathbf{r}_\perp$ is influenced by a charge $Q$ moving with velocity $v$ in the expanding matter.

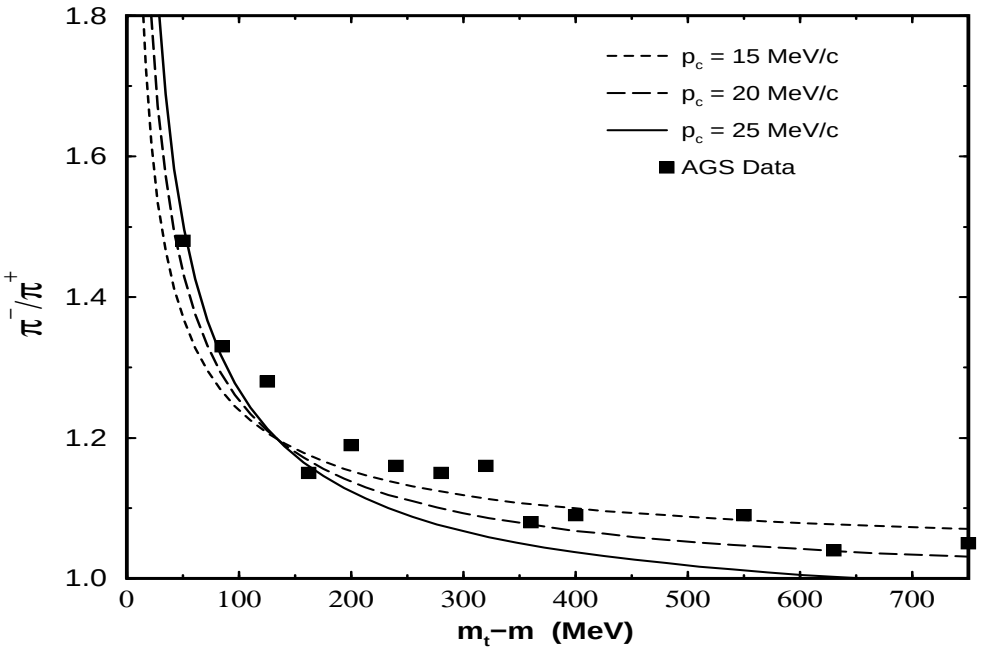


FIG. 3. Experimental $\pi^-/\pi^+$ ratios [4] for the reactions $Au + Au$ at 11.6 AGeV as a function of transverse mass compared to calculations employing Eq. (13) using a constant momentum shift $p_c$.

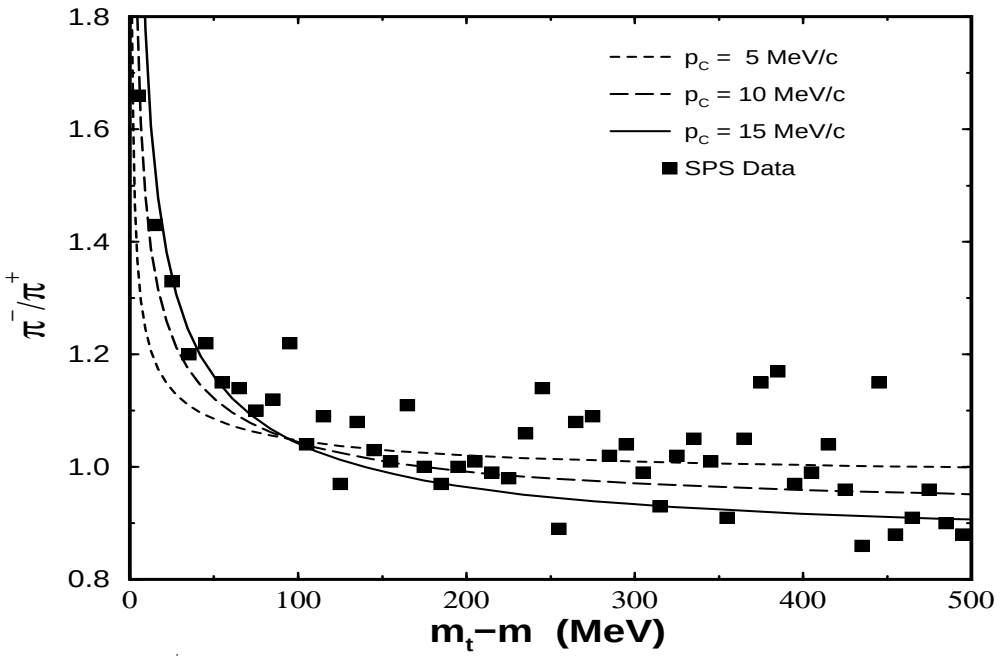


FIG. 4. Experimental $\pi^-/\pi^+$ ratios [5] at SPS energies for the reaction $Pb + Pb$ as a function of transverse mass compared to calculations using Eq. (13) using a constant momentum shift $p_c$.

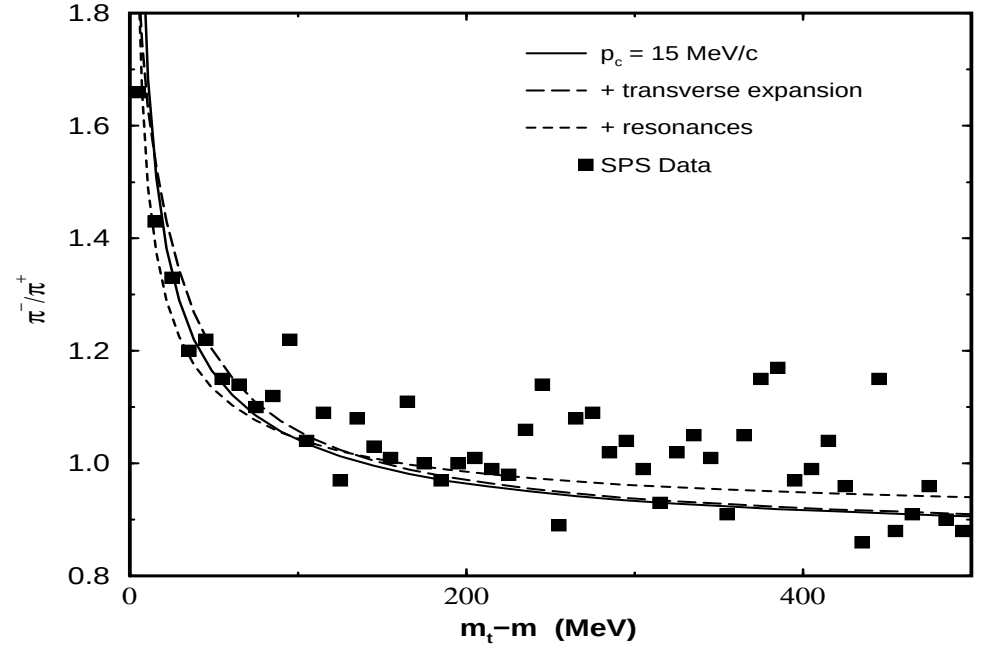


FIG. 5. The effect of resonances and transverse expansion on $\pi^-/\pi^+$ ratios Eq. (13) (see Fig. 4 and text).

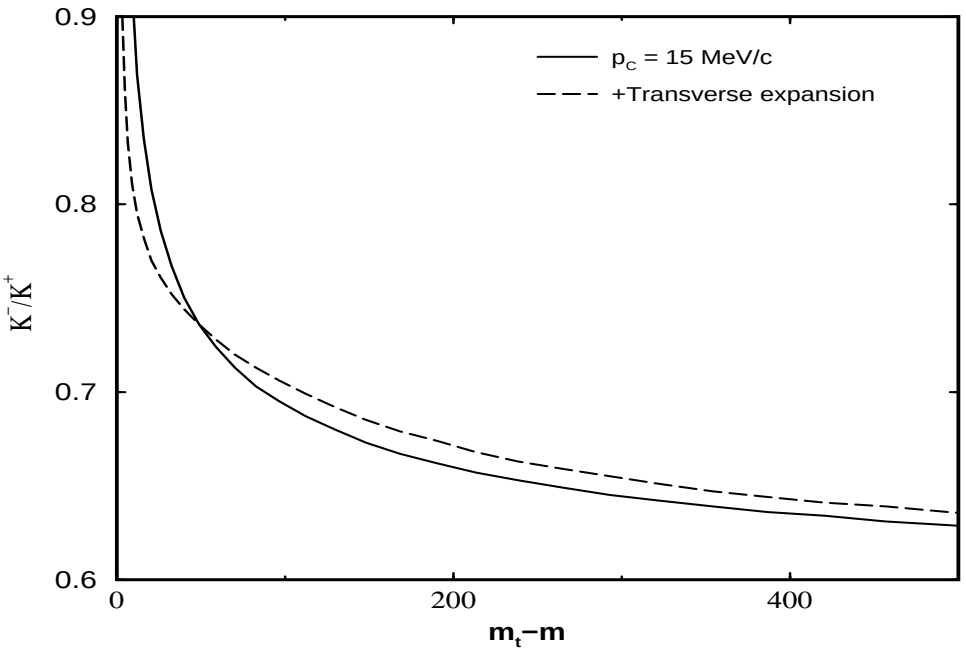


FIG. 6. The predicted $K^-/K^+$ ratios at SPS energies for the reaction $Pb + Pb$ as a function of transverse mass from Eq. (13) with $\Delta p_\perp = 15$ MeV/c (full curve). Dashed curve includes transverse expansion of Eq. (16).

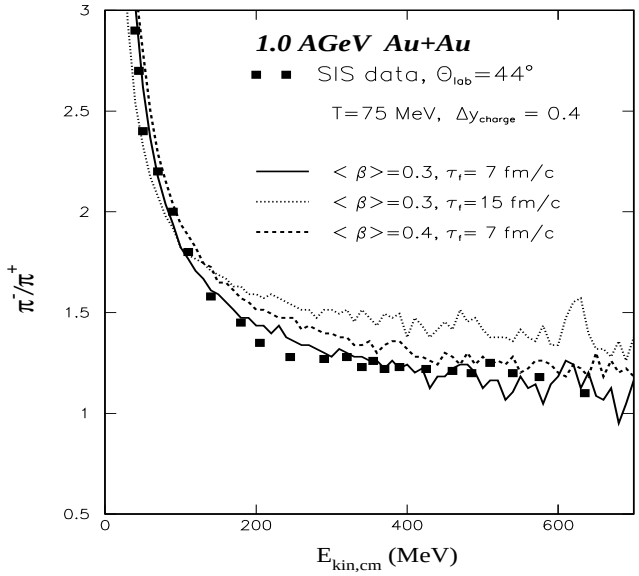

FIG. 7. Calculations of $\pi^-/\pi^+$ ratios with the dynamical model for the reactions $Au + Au$ at 1.0 AGeV as a function of pion kinetic energy in the center-of-mass system compared to experiment [2]. Good agreement is obtained with $\tau = 10fm/c$ for a moderate mean flow velocity $\langle\beta\rangle = 0.3$ c or $\tau = 7fm/c$ for $\langle\beta\rangle = 0.4$ c.

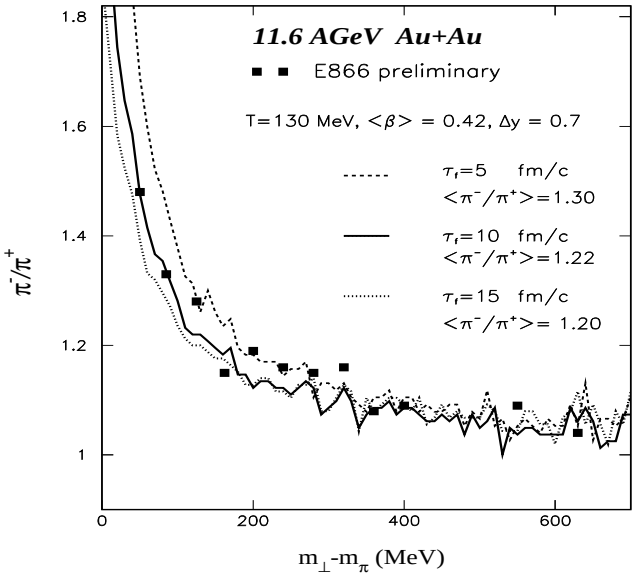


FIG. 8. Experimental $\pi^-/\pi^+$ ratios [4] for the reactions $Au + Au$ at 11.6 AGeV as a function of transverse mass compared to calculations using the dynamical Coulomb model for different freeze-out times $\tau_f$.

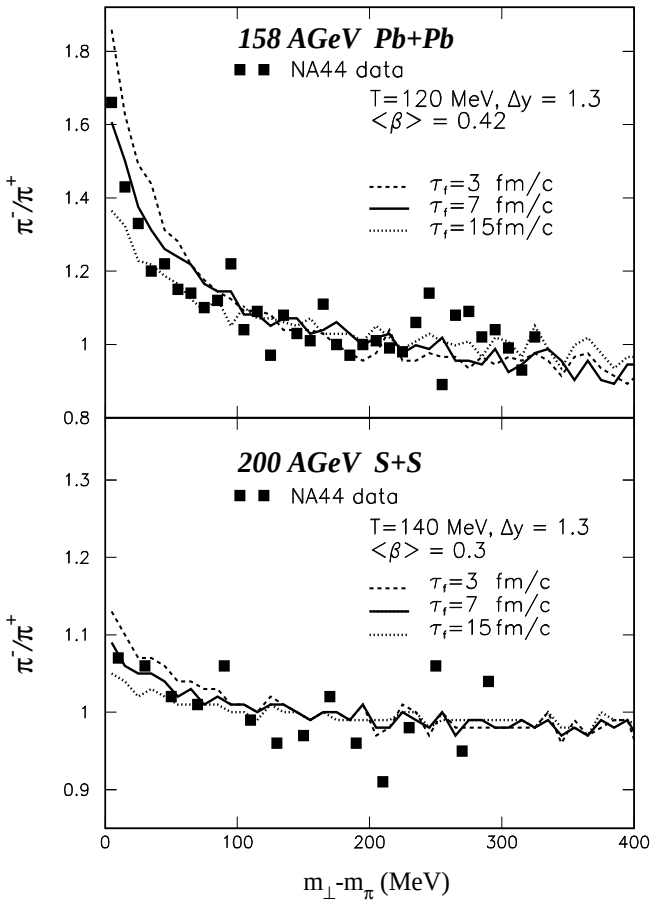


FIG. 9. Experimental $\pi^-/\pi^+$ ratios [5] at SPS energies for the reactions $Pb + Pb$ and $S + S$ as a function of transverse mass compared to calculations employing the dynamical Coulomb model with three different values for the freeze-out time.

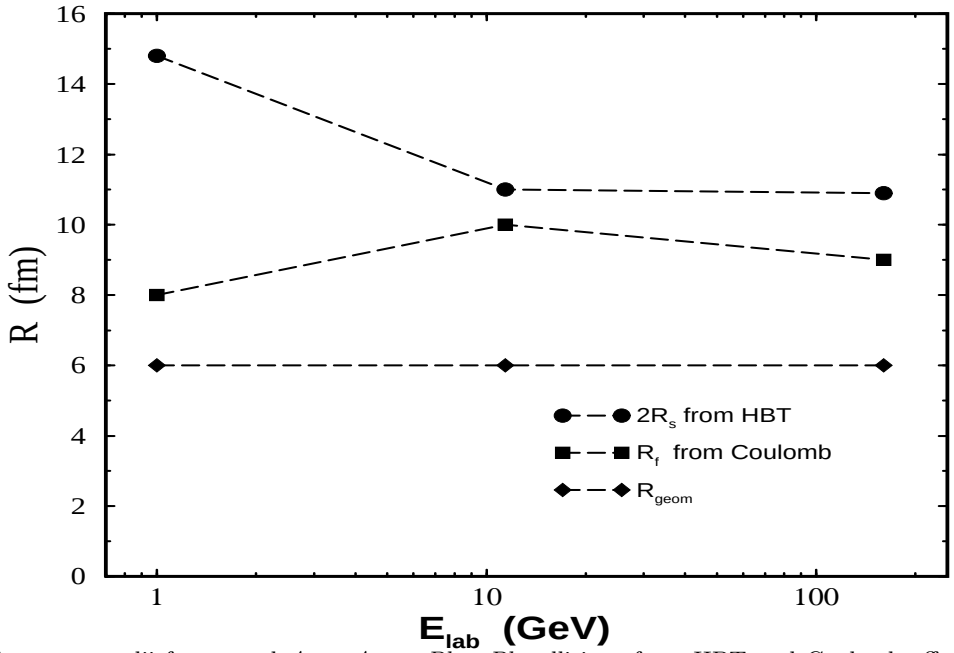


FIG. 10. The freeze-out radii for central $Au + Au$ or $Pb + Pb$ collisions from HBT and Coulomb effects. The HBT data are average values of $\pi^+\pi^+$ and $\pi^-\pi^-$ sideward HBT radii taken from Refs. [28], [29] and [25,31,32] at SIS, AGS and SPS energies respectively. The radii extracted from Coulomb effects are compatible with those from HBT except at SIS energies. The geometrical radii of the overlap zones (for $\sim 14\%$ centrality) at time of collision are smaller indicating that significant expansion takes place between collision and freeze-out.

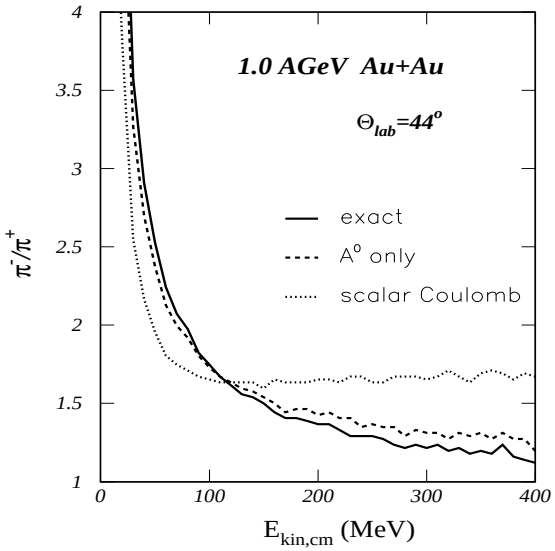


FIG. 11. $\pi^-/\pi^+$ ratios for Au on Au collisions at 1 AGeV as a function of the center-of mass kinetic energy calculated with the correct retarded electromagnetic potential (solid line) in comparison with an approximative treatment retaining only the time component without retardation (dashed line) and using a simple scalar Coulomb potential (dotted line).

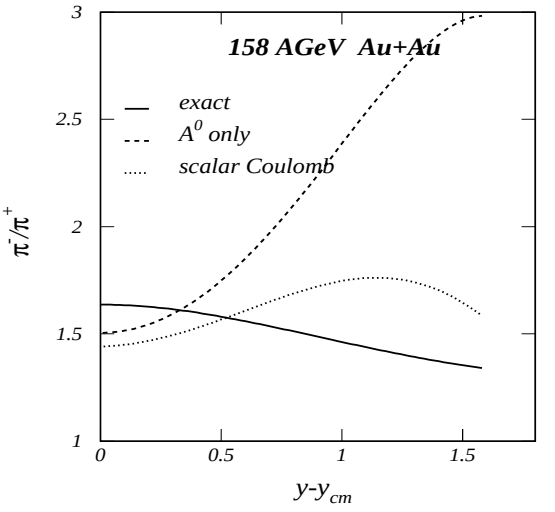


FIG. 12. $\pi^-/\pi^+$ ratios for Pb on Pb collisions at 158 AGeV at transverse kinetic energies smaller than 10 MeV calculated with the correct potential and two approximations (see caption of Fig. 11).